# Supporting Information

## Asymmetry and Bromination Strategies in the Design of Self-Assembled Monolayers for High-Performance Organic Solar Cells

Sinan Lu,[a] Shuyi Zhang,[a] Yi Li,[a] Fangcong Zhang,[a] Huiting Fu*[ab] and Qingdong Zheng*[a]

[a] State Key Laboratory of Coordination Chemistry, College of Engineering and Applied Sciences, Nanjing University, Nanjing 210023, China

*E-mail: zhengqd@nju.edu.cn; fuhuiting@nju.edu.cn

[b] Shenzhen Research Institute of Nanjing University, Shenzhen 518057, China

## Experimental Section

### Materials

All the materials were used without further purification. PEDOT:PSS were purchased from Xi'an Yuri Solar Co., Ltd. D18 was purchased from HYPER Material Inc. PM6, BTP-eC9, Y6, LB-BO and PNDIT-F3N were purchased from Solarmer Material Inc. 11H-Benzo[a]carbazole were purchased from Beijing InnoChem Science & Technology Co., Ltd. 5,8-Dibromo-11H-benzo[a]carbazole and diethyl (2-bromoethyl) phosphonate were purchased from Bide Pharmatech Ltd. Sodium hydride and trimethylbromosilane were purchased from Anhui Zesheng Technology Co., Ltd. 1,3,5-Trichlorobenzene (TCB) and 1,4-diiodobenzene (DIB) were purchased from Adamas-beta Ltd.

### Fabrication and Characterization of Devices

All devices in this work were fabricated with the structure of ITO/hole-selective layer/active layer/PNDIT-F3N/Ag. Pre-patterned indium tin oxide (ITO) glass substrates (sheet resistance of ≈12 Ω) were sonicated in detergent, deionized water, ethanol, and isopropanol for 30 min each sequentially and then dried at 70 ℃.

Subsequently, all substrates were treated with ultraviolet/ozone for 15 min. PEDOT:PSS (Heraeus Clevios P VP. AI 4083, filtered through a 0.45 $\mu$m filter) was spin-coated on the cleaned ITO substrates in ambient air and thermally annealed at 150 ℃ for 15 min to remove residual water. For SAM-based devices: a solution of BACz or 2Br-BACz (0.50 mg/mL in isopropanol) was applied onto the ITO substrate for 10 s, followed by spin-coating at 3000 rpm for 30 s. The ITO/SAMs substrate was then annealed on a hotplate and at 100 °C for 5 min, dynamically rinsed with isopropanol via spin-coating (3000 rpm, 30 s), and annealed again at 100 ℃ for 5 min.

The active layer solutions were prepared and processed under the following conditions: PM6:BTP-eC9 solution (1:1.2, 16.0 mg/mL in chloroform with 0.35 vol% 1,8-diiodooctane) was spin-coated at 2800 rpm for 30 s to obtain a ~100 nm thick film, then the PM6:BTP-eC9 film was annealed at 100°C for 10 min; PM6:Y6 solution (1:1.2, 14 mg/mL in chloroform with 0.50 vol% 1-chloronaphthalene) was spin-coated at 3000 rpm for 30 s, then the PM6:Y6 film was annealed at 80 °C for 5 min; PM6:L8-BO solution (1:1.2, 17.5 mg/mL in chloroform with 0.50 vol% 1,8-diiodooctane) was spin-coated at 3000 rpm for 30 s, then the PM6:L8-BO film was annealed at 100 °C for 10 min; D18:L8-BO solution (1:1, 9 mg/mL in chloroform with 5 mg/ml 1,4-diiodobenzene ) was spin-coated at 2100 rpm for 30 s, then the D18:L8-BO film was annealed at 100 °C for 10 min. PM6:M36 solution (1:1, 15 mg/mL in chloroform with 0.60 vol% 1-chloronaphthalene) was spin-coated at 3000 rpm for 30 s, then the PM6:M36 film was annealed at 85 °C for 5 min. Finally, PNDIT-F3N (0.5 mg/mL in methanol) was spin-coated at 2000 rpm onto the active layer and 120 nm of Ag was thermally evaporated to complete the device with an active area of 0.042 $cm^2$.

## *J-V* and EQE Measurement

Current density-voltage (*J-V*) characteristics were recorded with a Keithley 2400 Source Measure Unit under room temperature in the glove box. The photovoltaic performance was tested under AM 1.5G illumination at 100 mW $cm^{-2}$ using a solar simulator (Enlitech, SS-F5, Taiwan). The external quantum efficiency (EQE) spectra were obtained on a commercial EQE measurement system (Enlitech, QE-R). The light

intensity at each wavelength was calibrated by a standard single-crystal Si photovoltaic cell.

## Measurement of Mobility

Hole and electron mobilities were measured using the space-charge-limited-current (SCLC) method. Hole-only devices were fabricated with ITO/HSL/active layer/$MoO_3$/Ag, while electron-only devices were prepared with ITO/ZnO/active layer/PNDIT-F3N/Al architecture. The active layers were prepared using the same method for the best-performance OSC fabrication. Device areas were fixed at 4.2 $mm^2$. A Keithley 2440 source measurement unit measured the current density ($J$). The SCLC hole/electron mobilities were calculated according to the following equation:

$$J = \frac{9}{8}\varepsilon_0\varepsilon_r\mu\frac{V^2}{L^3}$$

where $J$ is the current density, $\varepsilon_0$ is the free-space permittivity ($8.85 \times 10^{-12}$ F $m^{-1}$), and $\varepsilon_r$ is the relative dielectric constant of the active layer material, usually 2-4 for organic semiconductors, herein we used a relative dielectric constant of 3, $\mu$ is the mobility of hole or electron, $V$ is the voltage drop across the SCLC device ($V = V_{app}$-$V_{bi}$, where $V_{app}$ is the applied voltage to the device and $V_{bi}$ is the built-in voltage due to the difference in the work function of two electrodes, in the hole- and electron-only devices, the $V_{bi}$ values are 0.5 and 0.7 V, respectively), and $L$ is the thickness of the active layer. The active layer thickness was detected by a Bruker Dektak XT surface profilometer.

## Theoretical Calculations

All the calculations of the model compounds studied in this work were performed using the Gaussian 09 software package. Ground state geometry optimizations of BACz and 2Br-BACz were calculated by DFT at the B3LYP/6-311G (d, p) (empirical dispersion=gd3bj) level. Then the ESP characteristic parameters were calculated based on the optimal structure with electronic wave function information using Multiwfn 3.8 (dev) program. The visualization of the molecular orbitals and ESP distribution was performed using Gauss View 5.0.9.

Adsorption energy calculations for all ITO surfaces were performed using the Material Studio software package on the basis of DFT theory. Under the Castep module, the generalised-gradient approximation (GGA) containing the Perdew-Burke-Emzerhof (PBE) with the proposed Newtonian algorithm of the LBFGS was used to optimize the 2BrBACz, BACz, and the cellular of ITO The models were structurally optimized separately with the default convergence limit set to $10^{-5}$ eV/atom. After the cut surface (111) and cell expansion operations of the ITO cell were completed, the vacuum layer was set to 20 Å. Then the molecules were placed on the (111) crystalline surface of the ITO respectively, and the truncation energy was chosen to be 500 eV and the free movement of atoms was allowed. After all the structural optimizations converged, single point energy calculations were performed for each substance. The adsorption energy was calculated as $E_{absorption} = E_{ITO@SAM} - E_{ITO(111)} - E_{SAM}$, where the more negative the value of $E_{absorption}$, the more tightly the molecules are adsorbed to the surface.

## Measurements of absorption spectra and cyclic voltammetry (CV)

UV-vis absorption spectra were obtained from a Shimadzu spectrophotometer. Cyclic voltammetry (CV) measurement was performed on a CHI-604E electrochemical workstation with a three-electrode cell in a nitrogen-bubbled 0.1 M tetrabutylammonium hexafluorophosphate ($Bu_4NPF_6$) solution in acetonitrile at a scan rate of 100 mV $s^{-1}$ at room temperature.

## Synthesis

The synthetic routes for the two SAM molecules are illustrated in **Scheme S1**. 11H-Benzo[a]carbazole (1a), 5,8-dibromo-11H-benzo[a]carbazole (2a) and diethyl (2-bromoethyl)phosphonate were purchased from BIDE Pharm. All chemicals were used as received without further purification.

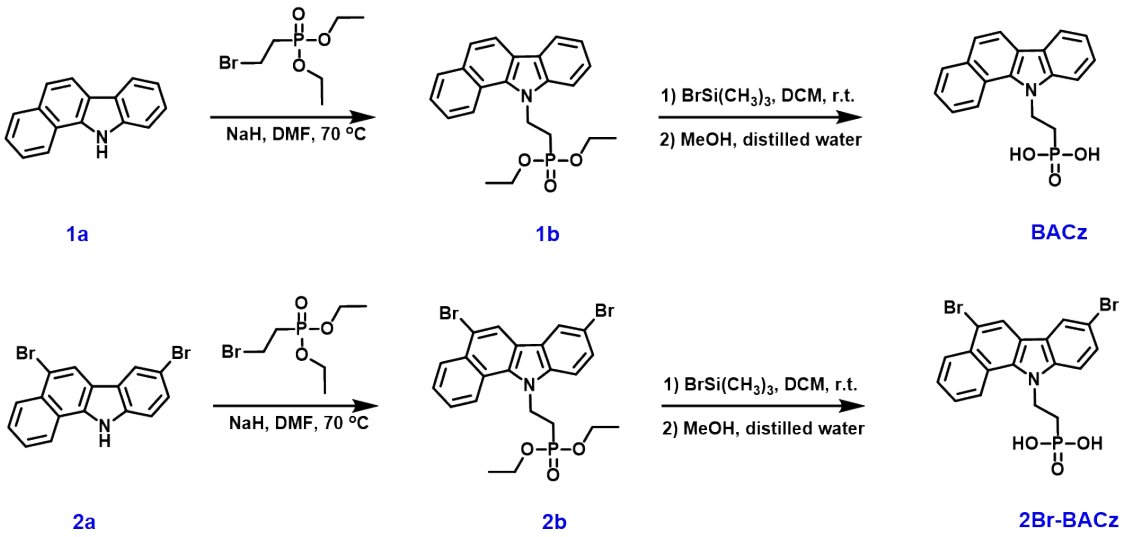


**Scheme S1**. Synthetic routes to BACz and 2Br-BACz.

**Synthesis of diethyl (2-(11H-benzo[a]carbazole-11-yl)ethyl)phosphonate (1b)**

Compound 1a (0.50 g, 2.30 mmol) and NaH (92.05 mg, 2.30 mmol) were dissolved in 30 mL anhydrous DMF under room temperature and stirred for 10 min under $N_2$ atmosphere. Then, diethyl (2-bromoethyl) phosphonate (0.56 g, 2.30 mmol) was added via syringe and the mixture was heated at 70 °C for 4 h. Afterwards, the reaction mixture was poured into 100 mL NaCl aqueous solution and extracted with ethyl acetate (EA) three times. The organic phase was dried over with anhydrous $Na_2SO_4$, and concentrated under reduced pressure to obtain the crude product. The crude product was purified by silica gel chromatography (eluent, petroleum ether: ethyl acetate = 1:3) to afford a white solid of compound 1b (0.68 g, yield 77%). $^1$H NMR (400 MHz, $CDCl_3$):8.54 (d, $J$ =8.5 Hz, 1H), 8.16 (t, 2H), 8.05 (d, $J$ =6.7 Hz, 1H), 7.68 (d, $J$ =8.5 Hz, 1H), 7.64-7.59 (m, 2H), 7.56-7.49 (m, 2H), 7.33 (t, 1H), 5.14-5.09 (m, 2H), 4.26-4.12 (m, 4H), 2.50-2.42 (m, 2H), 1.40-1.37 (m, 6H). $^{13}$C NMR (125 MHz, $CDCl_3$):139.75, 133.88, 133.64, 129.79, 125.83, 125.05, 124.72, 123.31, 122.12, 121.43, 121.06, 120.02, 119.77, 119.67, 119.17, 108.88, 62.08, 62.01, 40.13, 27.37, 16.56, 16.50.

**Synthesis of (2-(11H-benzo[a]carbazole-11-yl)ethyl)phosphonic acid (BACz)**

Compound 1b (0.50 g, 1.31 mmol) was dissolved in 30 mL anhydrous dichloromethane at room temperature under $N_2$ atmosphere. Then, bromothrimethylsilane (2.01 g, 13.1 mmol) was dropped, and the mixture was stirred for 24 h. Afterwards, 10 mL methanol was added to the mixture, and stirred for 10 min. The mixture was concentrated under

reduced pressure until approximately 5 mL of solution remains. Finally, distilled water was dropped slowly until a large amount of solid was produced. The solid was filtered off and washed with water to afford a white solid of BACz (0.29 g, 67%). $^{1}$H NMR (400 MHz, $d_6$-DMSO): 8.63 (d, $J$ =8.4 Hz, 1H), 8.31-8.25 (m, 2H), 8.12 (d, $J$ =6.7 Hz, 1H), 7.74-7.64 (m, 3H), 7.60 (t, 1H), 7.53 (t, 1H), 7.31 (t, 1H), 5.04-5.00 (m, 2H), 2.28-2.09 (m, 2H). $^{13}$C NMR (125 MHz, $d_6$-DMSO):139.87, 133.85, 133.61, 129.91, 126.45, 125.57, 125.36, 122.92, 122.17, 122.01, 121.05, 120.26, 120.23, 119.79, 119.21, 109.74, 40.65, 29.77. HRMS (ESI) m/z: $[M-H]^-$ calcd. for $C_{18}H_{16}NO_3P$, 324.0789; found, 324.0799.

**Synthesis of diethyl (2-(5, 8-dibromo-11H-benzo[a]carbazole-11-yl)ethyl) phosphonate (2b)**

Compound 2b (0.51 g, 81%) was synthesized following a procedure similar to that for the synthesis of 1b using compound 2a (0.50 g, 1.33 mmol), NaH (53.33 mg, 1.33 mmol) and diethyl (2-bromoethyl)phosphonate (0.33 g, 1.33 mmol) as the reactants. The resulting colorless liquid was purified by silica gel chromatography (eluent, petroleum ether:ethyl acetate=1:3). $^{1}$H NMR (400 MHz, $CDCl_3$): 8.47-8.44 (m, 2H), 8.35 (s, 1H), 8.14 (d, $J$ =1.8 Hz, 1H), 7.66-7.59 (m, 2H), 7.55-7.52 (m, 1H), 7.42 (d, $J$ =8.8 Hz, 1H), 5.03-4.97 (m, 2H), 4.16-4.03 (m, 4H), 2.39-2.30 (m, 2H), 1.31-1.27 (m, 6H). $^{13}$C NMR (125 MHz, $CDCl_3$): 138.47, 133.87, 131.11, 129.24, 128.25, 126.81, 126.31, 124.00, 123.08, 122.93, 122.36, 121.68, 119.01, 114.65, 113.35, 110.65, 62.16, 62.10, 40.37, 27.20, 16.54, 16.48.

**Synthesis of (2-(5, 8-dibromo-11H-benzo[a]carbazole-11-yl)ethyl)phosphonic acid (2Br-BACz)**

2Br-BACz (0.27 g, 61%) was synthesized following a procedure similar to that for the synthesis of BACz using compound 2b (0.50 g, 0.93 mmol) and bromotrimethylsilane (1.42 g, 9.30 mmol) as the reactants. $^{1}$H NMR (400 MHz, $d_6$-DMSO): 8.23 (d, $J$ =8.1 Hz, 1H), 7.91 (d, $J$ =9.6 Hz, 1H), 7.62 (t, 2H), 7.51 (t, 1H), 7.47 (d, $J$ =3.1 Hz, 1H), 7.38 (t, 1H), 7.05 (d, $J$ =3.1 Hz, 1H), 4.48-4.42 (m, 2H), 2.15-2.07 (m, 2H). $^{13}$C NMR

(125 MHz, $d_6$-DMSO): 138.85, 134.15, 130.68, 128.56, 128.48, 127.55, 127.28, 124.25, 123.92, 123.09, 123.06, 123.00, 118.83, 113.75, 112.95, 112.24, 41.52, 29.53. HRMS (ESI) m/z: $[M-H]^-$ calcd. for $C_{18}H_{14}Br_2NO_3P$, 481.8979; found, 481.8981.

**Figure S1**. $^1H$ NMR spectrum of 1b in $CDCl_3$.

**Figure S2**. $^{13}C$ NMR spectrum of 1b in $CDCl_3$.

**Figure S3**. $^1H$ NMR spectrum of BACz in $d_6$-DMSO.

**Figure S4**. $^{13}C$ NMR spectrum of BACz in $d_6$-DMSO.

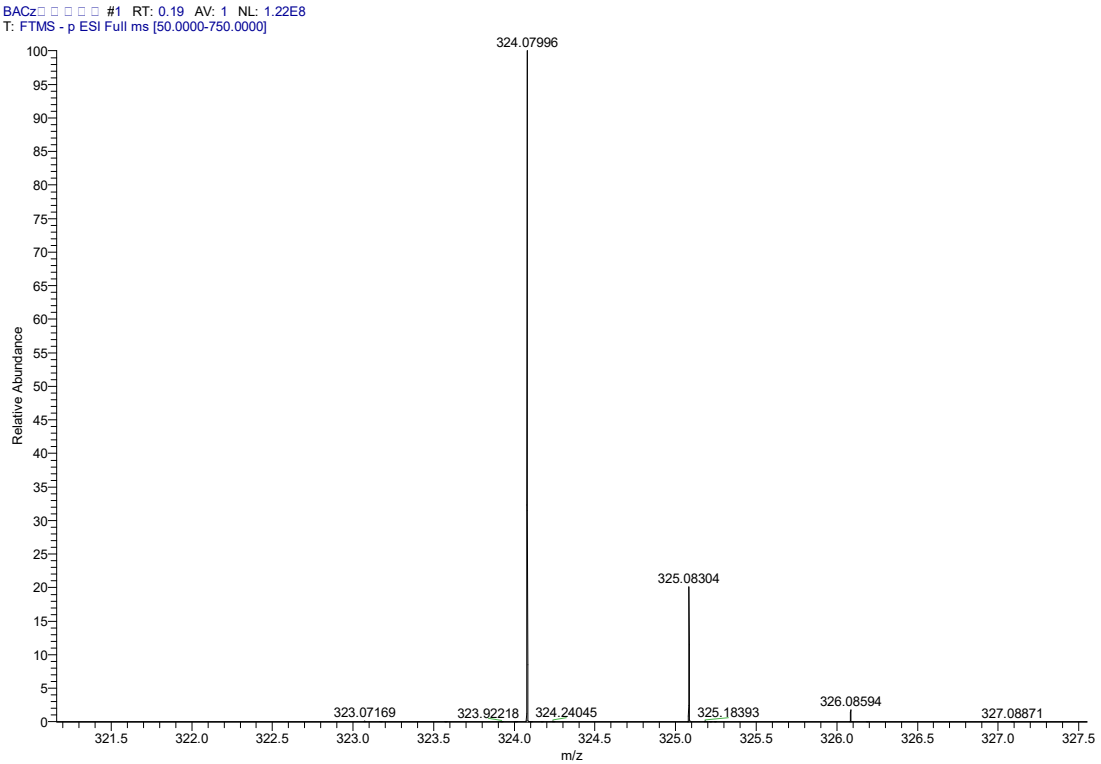


**Figure S5**. HRMS spectrum of BACz.

**Figure S6**. $^1H$ NMR spectrum of 2b in $CDCl_3$.

**Figure S7**. $^{13}C$ NMR spectrum of 2b in $CDCl_3$.

**Figure S8**. $^{1}H$ NMR spectrum of 2Br-BACz in $d_6$-DMSO.

**Figure S9**. $^{13}C$ NMR spectrum of 2Br-BACz in $d_6$-DMSO.

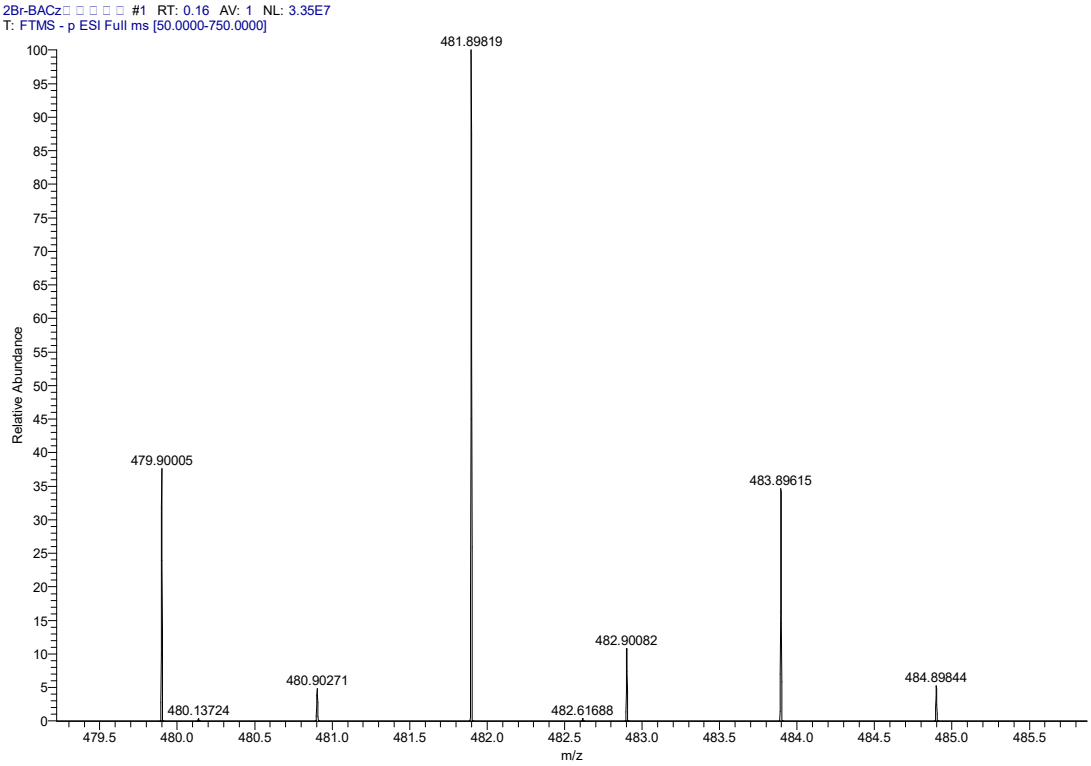


**Figure S10**. HRMS spectrum of 2Br-BACz.

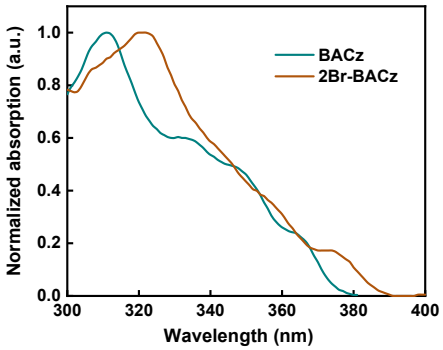


**Figure S11**. Absorption spectra of BACz and 2Br-BACz in films.

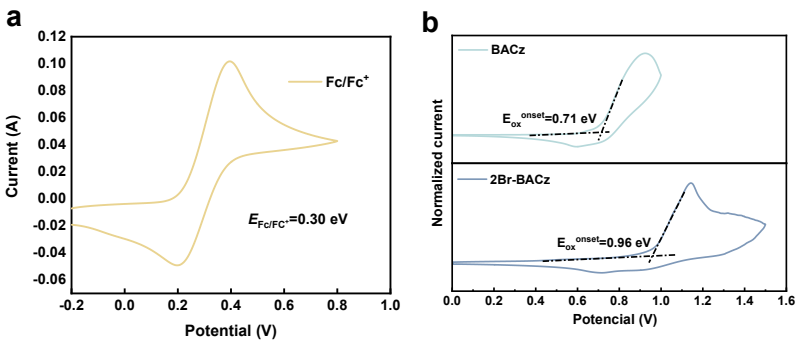


**Figure S12**. Cyclic voltammograms of a) $Fc/Fc^+$ and b) SAM molecules.

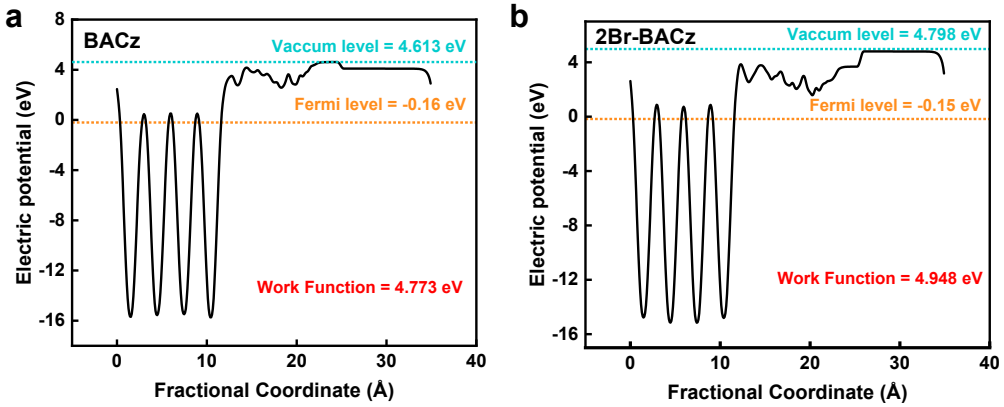


**Figure S13.** The electrostatic potential of two SAMs on ITO (111).

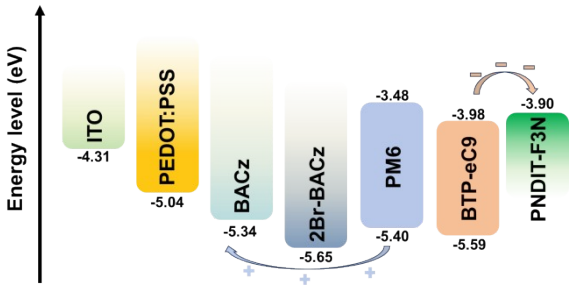


**Figure S14**. Schematic diagram of energy level arrangement.

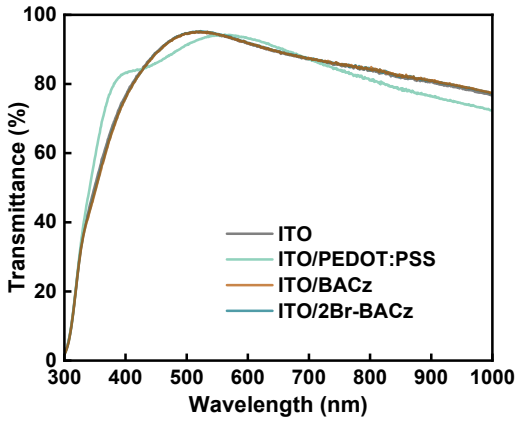


**Figure S15**. Transmittance spectra of ITO, ITO/PEDOT:PSS, ITO/BACz, and ITO/2Br-BACz substrates.

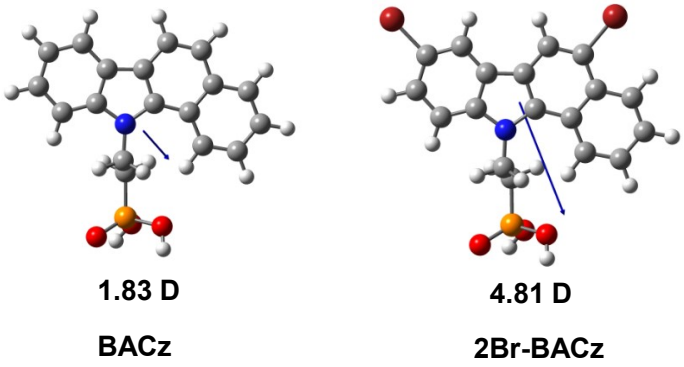


**Figure S16**. The calculated molecular structures and dipole moments of BACz and 2Br-BACz.

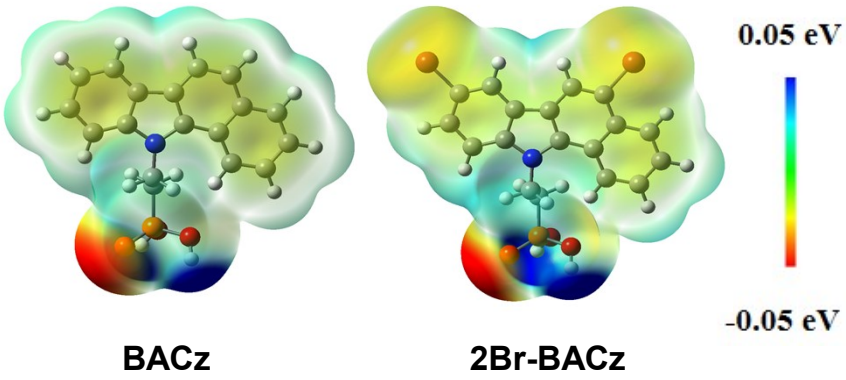


**Figure S17**. ESP distributions of BACz and 2Br-BACz.

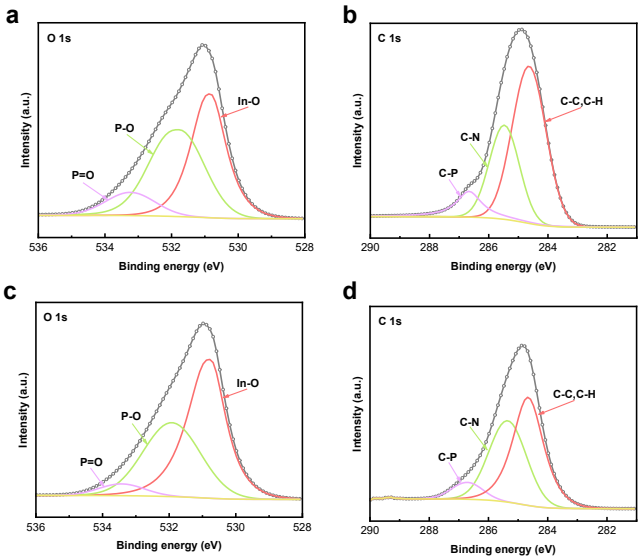


**Figure S18**. XPS of the C 1s and O 1s region of (a and b) ITO/BACz and (c and d) ITO/2Br-BACz.

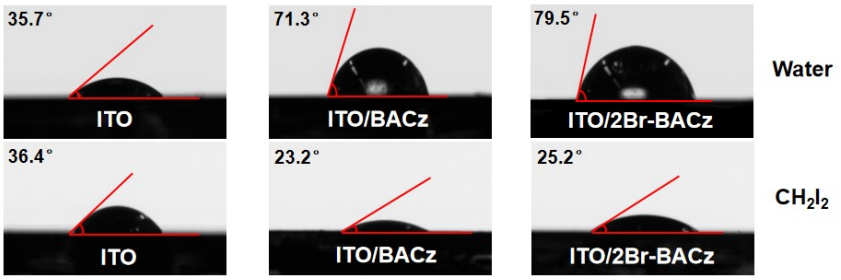


**Figure S19**. Contact angles measurements using water and diiodomethane.

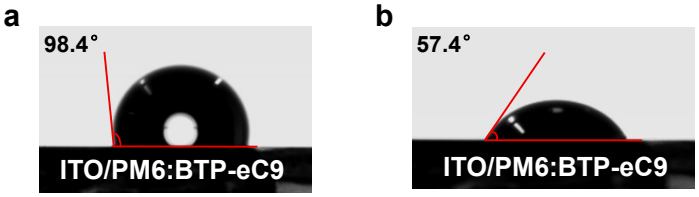


**Figure S20**. Contact angles of a) water and b) diiodomethane on ITO/PM6:BTP-ec9.

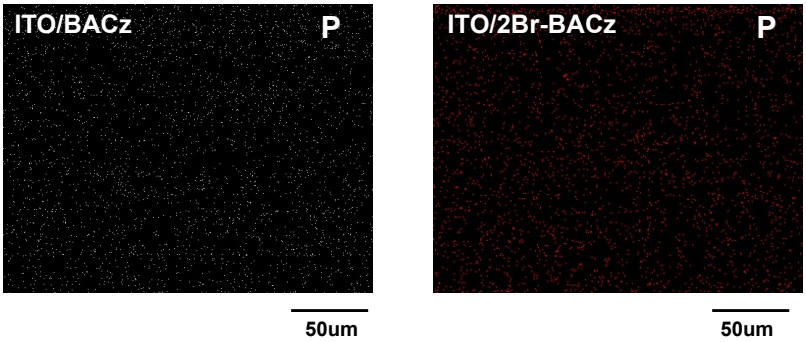


**Figure S21**. The elemental mapping of P for BACz and 2Br-BACz-modified ITO.

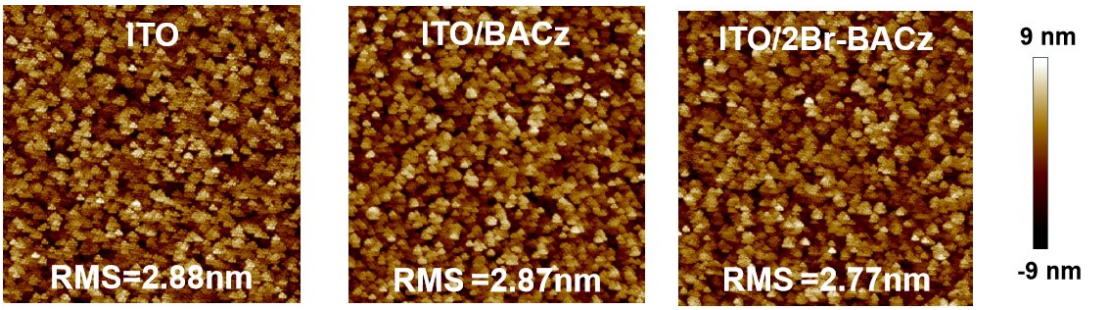


**Figure S22**. Atomic force microscopy height images for the bare ITO, ITO/BACz, and ITO/2Br-BACz.

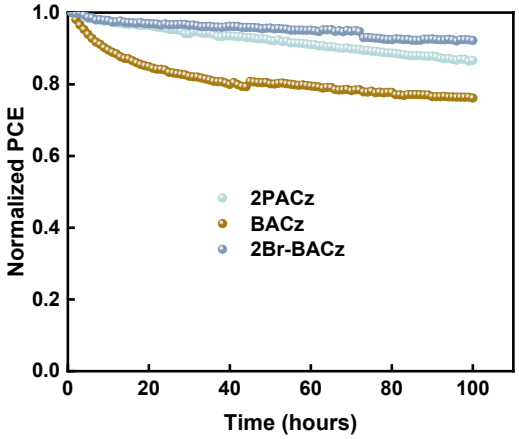


**Figure S23**. Photo-stability for PM6:BTP-eC9 devices based on different SAMs.

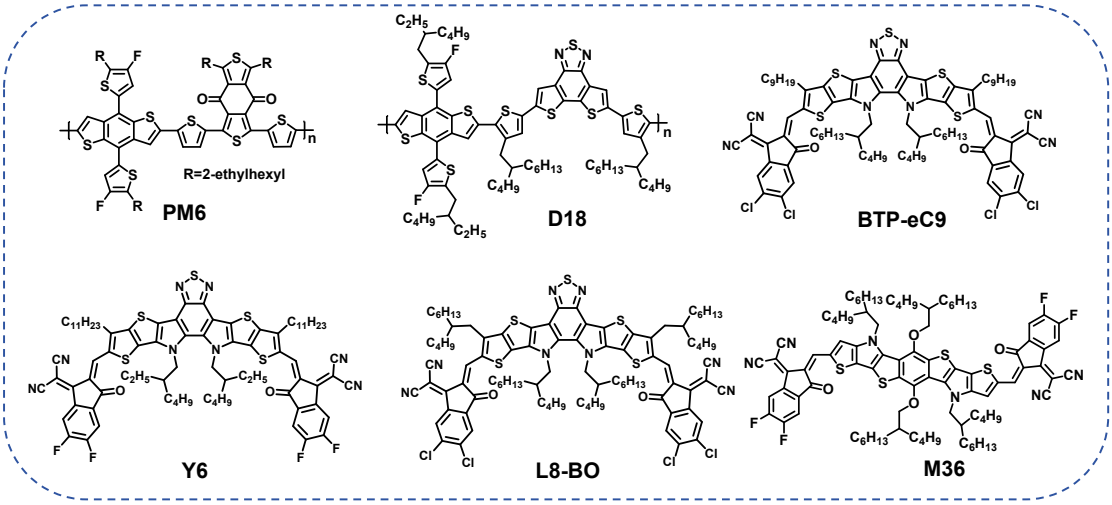


**Figure S24**. Chemical structures of the active layer materials used in this study.

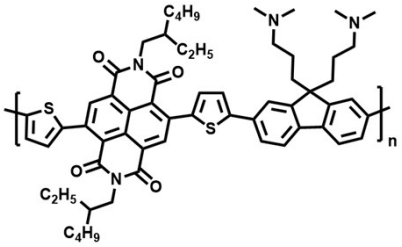

**Figure S25**. The chemical structure of the electron-selective layer PNDIT-F3N.

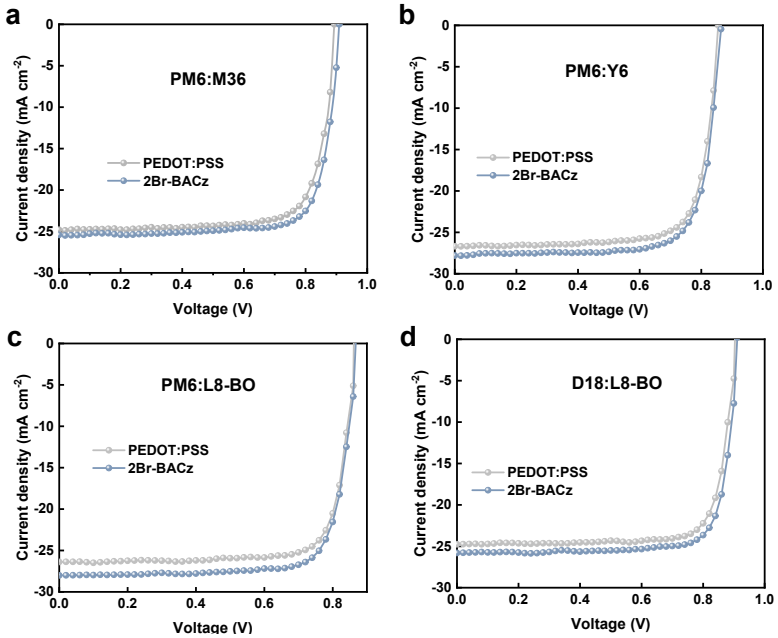


**Figure S26**. *J-V* curves of a) PM6:M36-, b) PM6:Y6-, c) PM6:L8-BO-, and d) D18:L8-BO-based OSCs with different HSLs.

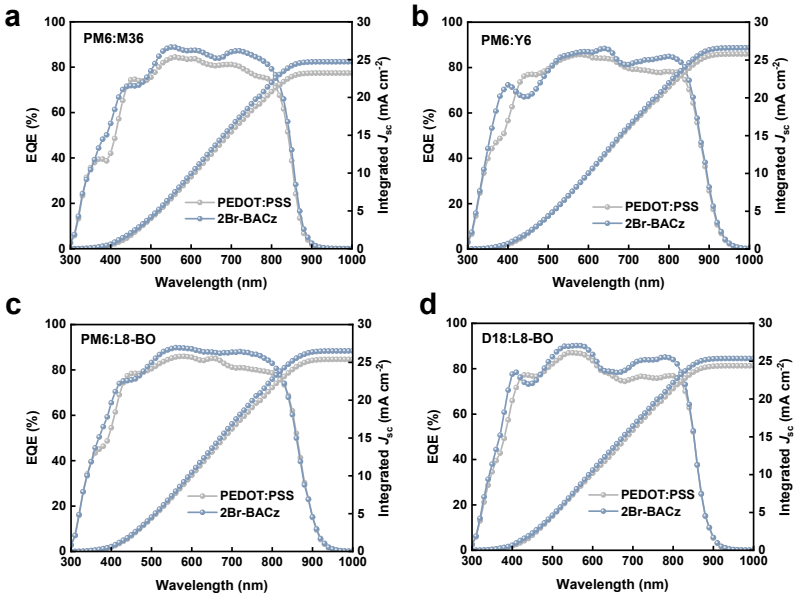


**Figure S27**. EQE spectra of a) PM6:M36-, b) PM6:Y6-, c) PM6:L8-BO-, and d) D18:L8-BO-based OSCs with different HSLs.

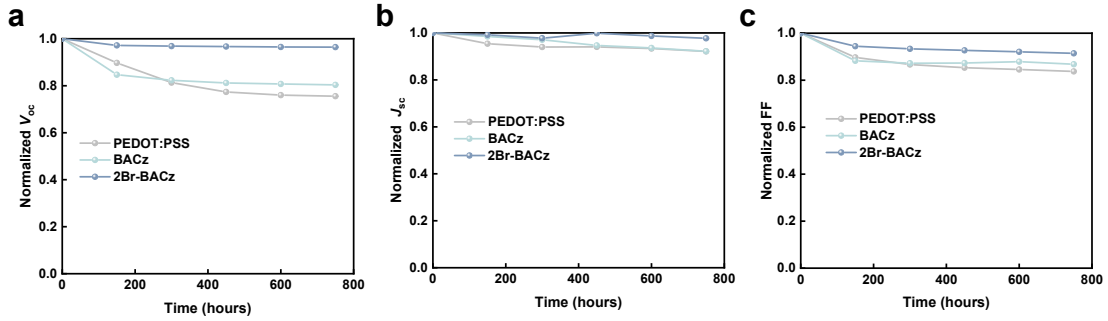


**Figure S28**. Variation of normalized a) $V_{oc}$, b) $J_{sc}$, and c) FF losses for PM6:BTP-eC9-based OSCs with different HSLs under continuous illumination at maximum power point.

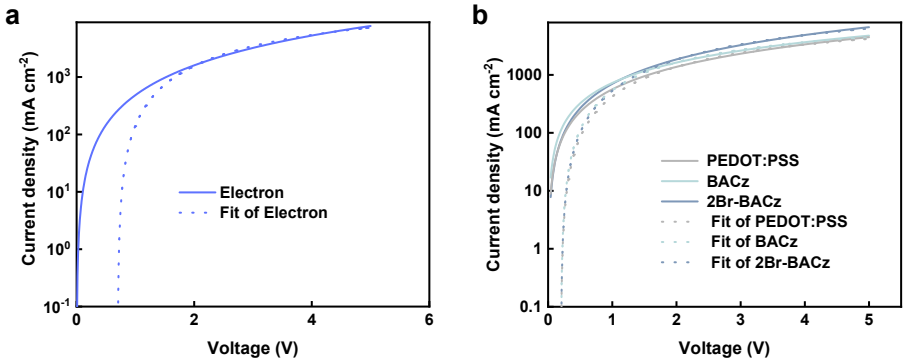


**Figure S29**. *J-V* curves for the a) electron-only and b) holy-only devices based on PEDOT:PSS, BACz, and 2Br-BACz.

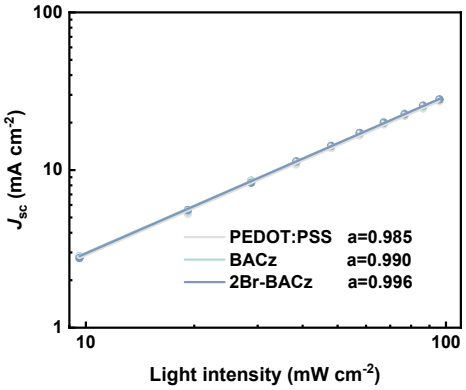


**Figure S30**. $J_{sc}$ *versus* $P_{light}$ plots for PEDOT:PSS-, BACz-, and 2Br-BACz-based devices.

**Table S1**. HOMO energy levels of SAMs.

| SAMs | HOMO (UPS) (eV) | HOMO (CV) (eV) | HOMO (DFT) (eV) |
|---|---|---|---|
| BACz | -5.34 | -5.47 | -5.56 |
| 2Br-BACz | -5.65 | -5.72 | -5.84 |

**Table S2**. Contact angles and surface tensions for different substrates.

| Substrates | $^{water}$ (°) | $^{CH2I2}$ (°) | $\gamma^d$ (mN m$^{-1}$) | $\gamma^p$ (mN m$^{-1}$) | $\gamma$ (mN m$^{-1}$) |
|---|---|---|---|---|---|
| ITO | 35.7 | 36.4 | 28.4 | 33.0 | 61.5 |
| ITO/BACz | 71.3 | 23.2 | 41.6 | 6.3 | 48.0 |
| ITO/2Br-BACz | 79.5 | 25.2 | 43.2 | 3.0 | 46.2 |
| ITO/PM6:BTP:eC9 | 98.4 | 57.4 | 29.6 | 0.6 | 30.2 |

**Table S3**. A summary of reported PCE values for conventional OSCs based on SAMs.

| SAMs | Device structure | Active layer | PCE (%) | Ref. |
|---|---|---|---|---|
| 2PACz | ITO/SAM/BHJ/PFN-Br/Ag | PM6:BTP-eC9:$PC_{71}BM$ | 18.03 | 1 |
| Br-2PACz | ITO/SAM/BHJ/PFN-Br/Ag | PM6:BTP-eC9:$PC_{71}BM$ | 18.4 | 2 |
| Br-2EPT | ITO/SAM/BHJ/Phen-NaDPO/Ag | PM6:BTP-eC11 | 17.28 | 3 |
| Cl-2PACz | ITO/SAM/BHJ/PNDIT-F3N/Ag | PM6:BTP-eC9:BV | 18.9 | 4 |
| 4,5-Cl-2PACz | ITO/SAM/BHJ/PNDIT-F3N/Ag | PM6:BTP-eC9:L8-BO-F | 19.05 | 5 |
| 2PACz | ITO/SAM/BHJ/PDINN/Ag | PM6:BTP-eC9:L8-BO | 20.17 | 6 |
| 4PADCB | ITO/SAM/BHJ/PNDIT-F3N/Ag | D18:L8-BO | 19.02 | 7 |
| Th-Cz | ITO/SAM:BHJ/$C_{60}$/BCP/Ag | D18-Cl:N3:AT-$\beta$2O | 20.91 | 8 |
| Br-DECz | ITO/SAM/BHJ/PNDIT-F3N/Ag | PM6:BTP-eC9 | 19.67 | 9 |
| 4PAThCz | ITO/SAM/BHJ/PNDIT-F3N/Ag | D18:L8-BO:BTP-eC9 | 20.78 | 10 |
| 2Br-BACz | ITO/SAM/BHJ/PNDIT- | PM6:BTP-eC9 | 20.03 | This |

| | | | | |
|---|---|---|---|---|
| | F3N/Ag | | | work |

**Table S4.** Photovoltaic parameters of PM6:BTP-eC9 devices based on different SAMs under AM 1.5G illumination.

| HSLs | $V_{oc}$ (V) | $J_{sc}$ (mA cm$^{-2}$) | FF (%) | PCE (%) |
|---|---|---|---|---|
| 2PACz | 0.854 | 28.6 | 78.1 | 19.1 |
| BACz | 0.859 | 28.4 | 78.7 | 19.2 |
| 2Br-BACz | 0.875 | 28.3 | 80.9 | 20.0 |

**Table S5**. Summarized photovoltaic performance of the OSC devices based on different donor-acceptor blends.

| Active Layers | HSLs | $V_{oc}$ (V) | $J_{sc}$ (mA cm$^{-2}$) | FF (%) | PCE (%) |
|---|---|---|---|---|---|
| PM6:M36 | PEDOT:PSS | 0.893 | 24.9 | 76.2 | 16.9 |
| PM6:M36 | 2Br-BACz | 0.909 | 25.4 | 78.0 | 18.0 |
| PM6:Y6 | PEDOT:PSS | 0.855 | 26.7 | 76.7 | 17.6 |
| PM6:Y6 | 2Br-BACz | 0.864 | 27.8 | 76.4 | 18.4 |
| PM6:L8-BO | PEDOT:PSS | 0.863 | 26.4 | 79.3 | 18.1 |
| PM6:L8-BO | 2Br-BACz | 0.867 | 27.9 | 78.6 | 19.1 |
| D18:L8-BO | PEDOT:PSS | 0.904 | 24.7 | 79.9 | 17.8 |
| D18:L8-BO | 2Br-BACz | 0.911 | 25.8 | 80.2 | 18.8 |

**Table S6**. Summarized electron and hole mobilities for the devices with different HSLs.

| HSLs | $\mu_e$ (cm$^2$ V$^{-1}$ s$^{-1}$) | $\mu_h$ (cm$^2$ V$^{-1}$ s$^{-1}$) | $\mu_e/\mu_h$ |
|---|---|---|---|
| PEDOT:PSS | $5.61\times10^{-4}$ | $2.40\times10^{-4}$ | 2.34 |
| BACz | | $4.04\times10^{-4}$ | 1.39 |

| | | |
|---|---|---|
| 2Br-BACz | $4.37\times10^{-4}$ | 1.28 |

**Table S7**. Summary of the fitting parameter used to describe the Nyquist plots.

| Electrodes | $R_s$ (Ω) | $R_{rec}$ (Ω) |
|---|---|---|
| ITO/PEDOT:PSS | 33.2 | 4840 |
| ITO/BACz | 22.4 | 7860 |
| ITO/2Br-BACz | 19.8 | 8682 |

## References


1. Y. Lin, Y. Firdaus, F. H. Isikgor, M. I. Nugraha, E. Yengel, G. T. Harrison, R. Hallani, A. El-Labban, H. Faber, C. Ma, X. Zheng, A. Subbiah, C. T. Howells, O. M. Bakr, I. McCulloch, S. D. Wolf, L. Tsetseris and T. D. Anthopoulos, *ACS. Energy. Lett.*, 2020, **5**, 2935-2944.
2. Y. Lin, A. Magomedov, Y. Firdaus, D. Kaltsas, A. El-Labban, H. Faber, D. R. Naphade, E. Yengel, X. Zheng, E. Yarali, N. Chaturvedi, K. Loganathan, D. Gkeka, S. H. AlShammari, O. M. Bakr, F. Laquai, L. Tsetseris, V. Getautis and T. D. Anthopoulos, *ChemSusChem*, 2021, **14**, 3569-3578.
3. A. Ullah, K. H. Park, Y. Lee, S. Park, A. B. Faheem, H. D. Nguyen, Y. Siddique, K.-K. Lee, Y. Jo, C.-H. Han, S. Ahn, I. Jeong, S. Cho, B. Kim, Y. S. Park and S. Hong, *Adv. Funct. Mater.*, 2022, **32**, 2208793.
4. Y. Lin, Y. Zhang, J. Zhang, M. Marcinskas, T. Malinauskas, A. Magomedov, M. I. Nugraha, D. Kaltsas, D. R. Naphade, G. T. Harrison, A. El-Labban, S. Barlow, S. De Wolf, E. Wang, I. McCulloch, L. Tsetseris, V. Getautis, S. R. Marder and T. D. Anthopoulos, *Adv. Energy. Mater.*, 2022, **12**, 2202503.
5. Y. Wang, W. Jiang, S.-C. Liu, C.-T. Lin, B. Fan, Y. Li, H. Gao, M. Liu, F. R. Lin and A. K.-Y. Jen, *Adv. Energy. Mater.*, 2024, **14**, 2303354.
6. S. Guan, Y. Li, C. Xu, N. Yin, C. Xu, C. Wang, M. Wang, Y. Xu, Q. Chen, D. Wang, L. Zuo and H. Chen, *Adv. Mater.*, 2024, **36**, 2400342.
7. Y. Li, Z. Jia, P. Huang, T. Liu, D. Hu, Y. Li, H. Liu, X. Lu, S. Lu, X. Yin and Y. Yang, *Adv. Energy. Mater.*, 2024, **14**, 2304000.
8. H. Mou, Y. Yin, H. Chen, J. Xu, J. Ding, C. Ju, J. Zhu, Y. Wang, W. Chen, G. Xu, T. Zhang, J. Li, Y. Li and Y. Li, *J. Am. Chem. Soc.*, 2025, **147**, 21241-21251.
9. L. Liu, F. Yu, D. Hu, X. Jiang, P. Huang, Y. Li, G. Tian, H. Lei, S. Wu, K. Tu, C. Chen, T. Gu, Y. Chen, T. Duan and Z. Xiao, *Energy. Environ. Sci.*, 2025, DOI: 10.1039/D4EE04515G.
10. Y. Xie, J. Tian, X. Yang, J. Chen, S. Yu, D. Tang, X. Hu, Y. Sun and M. Lv, *Adv. Mater.*, 2025, DOI: 10.1002/adma.202502485.